



**HAL**  
open science

## Towards the determination of carbon dioxide retention in earthen materials

Sofia Arris-Roucan, Fionn McGregor, Antonin Fabbri, Céline Perlot-Bascoules

► **To cite this version:**

Sofia Arris-Roucan, Fionn McGregor, Antonin Fabbri, Céline Perlot-Bascoules. Towards the determination of carbon dioxide retention in earthen materials. *Building and Environment*, 2023, 239, pp.110415. 10.1016/j.buildenv.2023.110415 . hal-04145330

**HAL Id: hal-04145330**

**<https://hal.science/hal-04145330>**

Submitted on 22 Feb 2024

**HAL** is a multi-disciplinary open access archive for the deposit and dissemination of scientific research documents, whether they are published or not. The documents may come from teaching and research institutions in France or abroad, or from public or private research centers.

L'archive ouverte pluridisciplinaire **HAL**, est destinée au dépôt et à la diffusion de documents scientifiques de niveau recherche, publiés ou non, émanant des établissements d'enseignement et de recherche français ou étrangers, des laboratoires publics ou privés.

# Towards the determination of carbon dioxide retention in earthen materials

Sofia Arris-Roucan<sup>\*1</sup>, Fionn McGregor<sup>1</sup>, Antonin Fabbri<sup>2</sup>, and Céline Perlot<sup>1,3</sup>

<sup>1</sup>Université de Pau et des Pays de l'Adour, E2S UPPA, SIAME, Anglet, France

<sup>2</sup>LTDS, UMR 5513 CNRS, ENTPE, Université de Lyon, 69120 Vaulx-en-Velin, France

<sup>3</sup>IUF, Institut Universitaire de France, Paris, France

## Abstract

Thanks to its hygroscopic properties, raw earth can passively buffer indoor humidity. The high sorption properties of clay minerals present in earth also attract other molecules, such as carbon dioxide (CO<sub>2</sub>), this can potentially lead to indoor CO<sub>2</sub> buffering. It would improve air quality in buildings and their resilience towards mechanised ventilation systems. However, there is currently no protocol to evaluate this potential. This paper aims to present a innovative methodology based on thermogravimetric (TG) and calorimetric (DSC) analysis to characterise the interactions between clay and CO<sub>2</sub> at the microscopic scale by focusing on the dry state. Results show a CO<sub>2</sub> adsorption capacity of 134 mg/kg at 5000 ppm at 35°C associated with a reversible physisorption process and provides first evidence of a passive CO<sub>2</sub> regulation capacity of the indoor air. Determination of the adsorption enthalpies as a function of the amount adsorbed revealed high values (from -74 kJ/mol to -40 kJ/mol) which are characteristic of a strong energetic heterogeneity of the material.

## Keywords:

Indoor air quality, Earthen materials, Carbon dioxide adsorption, Adsorption enthalpy, Thermogravimetry, Differential Scanning Calorimetry.

---

<sup>\*</sup>Corresponding author: sofia.roucan@univ-pau.fr

# 1 Introduction

Indoor Air Quality (IAQ) has become an issue of concern in the building and construction sector for several years [1]. This has resulted in an increase in the number of scientific publications on the subject [2], but also in the recognition in the UN Agenda 2030 as one of the 17 Sustainable Development Goals. It has been shown that poor indoor air quality can have negative health effects, ranging from simple discomfort to severe pathologies [3]. However, in the context of climate change and resource depletion, significant changes have taken place in the way buildings are designed [4], making them more airtight than older buildings in order to improve their energy efficiency [5]. This air-tightness, coupled with the widespread use of synthetic building materials, contributes to higher pollutant concentrations indoors than those found outdoors [6]. This is of particular concern in high-income countries where people spend more than 90% of their time indoors, increasing exposure time to pollutants and associated health risks [7]. Thus, while buildings are primarily intended to enhance the well-being of occupants, they are associated with a range of hazards, which may be exacerbated by climate change [8]. It is therefore necessary to recognise the strong interdependence between indoor environmental quality, energy efficiency and health.

Among the many pollutants present in indoor air, carbon dioxide ( $\text{CO}_2$ ) has been the subject of numerous recent studies. The presence of this gas in indoor air is mainly due to human metabolism and its concentration is therefore strongly related to occupancy levels. While it used to be considered harmless to health, several studies have shown that even at concentrations considered to be low,  $\text{CO}_2$  can have a harmful impact on health, particularly on fragile populations (children, elderly, people with chronic illnesses) [9] [10]. These effects can range from cognitive impairment to chronic disease depending on the concentration and time of exposure [11] [12]. While the proposed limit for indoor air is 1000 ppm [13], in inadequately ventilated areas its concentration often exceeds this threshold, which has been measured in schools in Europe [14] [15].

One of the strategies being considered for the regulation of  $\text{CO}_2$  in air is the buffering of these concentrations through the adsorption of  $\text{CO}_2$  on adsorbent surfaces [16] [17]. Adsorption is the accumulation of particles (adsorbate, here  $\text{CO}_2$ ) at a surface (adsorbent, here earth-based construction material) due to the operation of surface forces. The reverse process is called desorption. Adsorption can be of two kinds: physisorption in which the forces involved are intermolecular forces (van der Waals forces) and chemisorption which results from chemical bond formation [18].

By addressing indoor air quality through a passive strategy, buildings could provide healthier environments for their occupants, while also reducing their energy consumption and improving their overall resilience [19]. The difficulty in implementing this technique lies in the fact that indoor air concentrations

50 are very low, that the material must be able to regenerate and thus release all or part of the CO<sub>2</sub> when  
51 the concentration drops and finally the presence of humidity in the air must not hinder the stability  
52 of the material. Several materials have been studied for this purpose, including: amine-impregnated  
53 silicas [20] [21], metal organic frameworks [22], zeolites [23] [24] and activated carbons [25]. However,  
54 the difficulty of preparing these materials, their cost, as well as their stability at high humidity could  
55 compromise their widespread use.

56 On the other hand, raw earth, a material widely used in particular for interior plastering, could present  
57 ideal characteristics for this type of application. Earthen materials are known for their hygroscopic  
58 properties on the regulation of indoor humidity and their thermal inertia for heat storage [26] [27].  
59 Through the presence of clay minerals and their microstructure they could regulate the concentration of  
60 CO<sub>2</sub> on the same principle as humidity. In addition, they are fulfilling a truly circular economy approach  
61 without affecting natural resources, the earth being sourced from waste (mainly excavation works) from  
62 the construction sector and can potentially be infinitely reused [28]. Some relevant publications on indoor  
63 air pollutants retention had already concluded that one of the most promising passive removal materials  
64 for indoor ozone control are clay-based plasters and clay paints [29] [30]. However, there is currently no  
65 protocol for determining whether raw earth could passively regulate CO<sub>2</sub> even though some research is  
66 ongoing [31][32][33].

67 In this context, the objective of this paper is to present a new experimental methodology, based on  
68 thermogravimetry (TG) and differential scanning calorimetry (DSC), to evaluate the potential of raw  
69 earth to buffer CO<sub>2</sub>. The experimental set-up, consisting of the TG-DSC apparatus, a gas mixer and a  
70 wet gas generator, allows the representation of a wide range of indoor environments. The measurement  
71 of the mass and heat flow variations enables the characterisation of the process taking place. As a first  
72 step in the understanding of this phenomenon are the interactions between the injected gas and the clay  
73 material, therefore only the dry state of the material will be presented and discussed in this paper.

## 74 **2 Material and Methods**

### 75 **2.1 Earth characterisation**

76 A single earth was selected for this study coming from the “Auvergne Rhône-Alpes” region in south-  
77 eastern France. It was collected from a centenarian rammed earth construction located in the city of  
78 “Dagneux” [34] and referenced as DAG. This earth was selected for this study because it has been  
79 extensively studied in previous work ([35] [36]) and its properties are well known. Furthermore, coming  
80 from a real construction, this earth is suitable to be used as a building material. The selected earth was

81 crushed and sieved at 5 mm. Its particle size distribution was determined according to the French Norms  
82 NF EN ISO 17892-4 [37]. The different properties determined are presented in table 1, in particular it  
83 revealed that the earth contains 18% of clay (particles lower than 2  $\mu m$ ). As clay minerals play a key  
84 role in adsorption mechanisms, to get more information about the activity of this clayey fraction the  
85 methylene blue value ( $MB$ ) was used as an indicator since methylene blue is preferentially absorbed by  
86 clays and organic materials. The methylene blue tests were carried out on the fraction below 80  $\mu m$  of  
87 this earth following the French Standard NF P 94-068 [38]. The ratio between  $MB$  and the clay content  
88 in the 0-80  $\mu m$  fraction of the earth enables the deduction of the clay activity index ( $A_{cb}$ ). Results given  
89 in Table 1 indicate that the clay fraction of DAG has normal activity.

90 Then, powder X-ray diffraction (XRD) was used to identify the mineralogical composition of the  
91 earth. It was performed on oriented aggregates using two preparations: air dried or natural and after  
92 glycolation. Swelling clay minerals were detected in DAG. This seems in accordance with the measured  
93 clay activity index. The detected swelling clay minerals were characterized as interlayered illite/smectite  
94 minerals.

95 Finally nitrogen adsorption/desorption was performed to investigate the small pores. Approximately  
96 3 g of earth (fraction below 2mm) was subjected to one nitrogen intrusion-extrusion cycle at a constant  
97 temperature of 77 K. This cycle consisted in the pressurisation of gaseous nitrogen up to the saturation  
98 value followed by depressurisation back to the initial value. Throughout the cycle, the amount of intruded  
99 nitrogen was continuously measured to determine the isothermal adsorption and desorption curves (see  
100 Fig.1). The BET theory in the range of 0.05 to 0.35  $p/p^0$  was applied to determine the specific surface  
101 area of the 0-2mm fraction which is found to be 13  $m^2/g$ , typical values for pure clay minerals are in  
102 range of 5-20  $m^2/g$  for kaolinite, between 100 and 200  $m^2/g$  for illite and less than 1000  $m^2/g$  for smectite  
103 [39]. The shape of the isotherm corresponds to a type II according to the IUPAC classification [40] which  
104 represent a non-porous or macroporous material. The presence of a type H3 hysteresis is usually given  
105 by non-rigid aggregates of plate-like particles such as clay minerals that expand during the cycle. It is  
106 therefore difficult to assess the pore size distribution since there is no rigid skeleton, the interlayer space  
107 of clay minerals can expand and adopt various size.

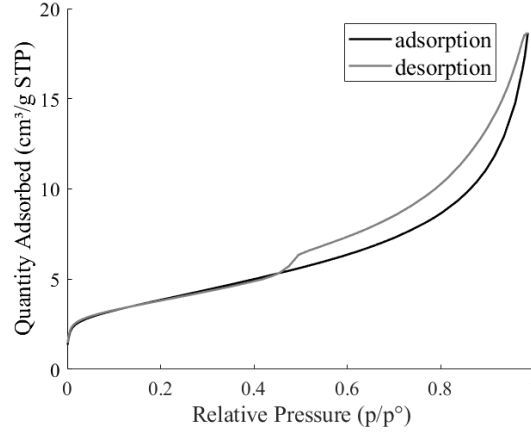


Figure 1: Nitrogen adsorption-desorption isotherm at 77 K for 3 g of DAG earth

108

Table 1: Main properties of DAG earth

Properties		Values
Geotechnical properties	Sand and fine gravel (5-0.06mm) [%]	27
	Silt (60-2 $\mu m$ ) [%]	55
	Clay (< 2 $\mu m$ ) [%]	18
	Methylene Blue value ( <i>MB</i> )	1.8
	Clay activity index ( $A_{cb}$ )	9.4
Main clay minerals	Smectite [%]	17.5
	Kaolinite [%]	10.1
Specific surface	0-2 mm fraction [ $m^2/g$ ]	13

109 Throughout the study, it is assumed that it is mainly the clay minerals in the earth that interact  
110 with the  $CO_2$ , as is the case with water. To maximise the phenomena, the choice was made to focus on  
111 the fine fraction of the earth, below 80  $\mu m$  which presents the highest surface area. The properties of  
112 the fraction below 80  $\mu m$  are very similar to the total fraction: the 0-80  $\mu m$  fraction contains 22% of  
113 sand and fine gravel, 59% of silt and 19% of clays. The nitrogen adsorption/desorption on that fraction  
114 and the application of the BET theory reveals a specific surface of 15.5  $m^2/g$ . Therefore, to work on this  
115 fine fraction, the earth was sieved at 80  $\mu m$  with the help of water. It was then heated to a maximal  
116 temperature of 95  $^\circ C$  for drying until constant mass was reached. Until testing, dried samples were  
117 stored in a box with silica gel.

## 2.2 Experimental set-up for carbon dioxide retention measurement

The general principle of the device is based on the coupling of a simultaneous thermal analysis with a wet gas generator and a CO<sub>2</sub>/air mixer. It allows the study of materials in a wide range of indoor like conditions by precisely controlling the relative humidity and CO<sub>2</sub> concentration. The general objective of the experiment is to qualify and quantify CO<sub>2</sub> and water retention capacities of an earthen material. For that purpose mass variation and heat flow of samples are measured as a function of the CO<sub>2</sub> concentration, relative humidity and temperature. The set-up is composed of: gas cylinders, gas mixer to select the desired CO<sub>2</sub> concentration, pressure regulator, wet gas generator, TG-DSC apparatus, CO<sub>2</sub> sensors as shown in Fig.2. The operation and role of each device is detailed below.

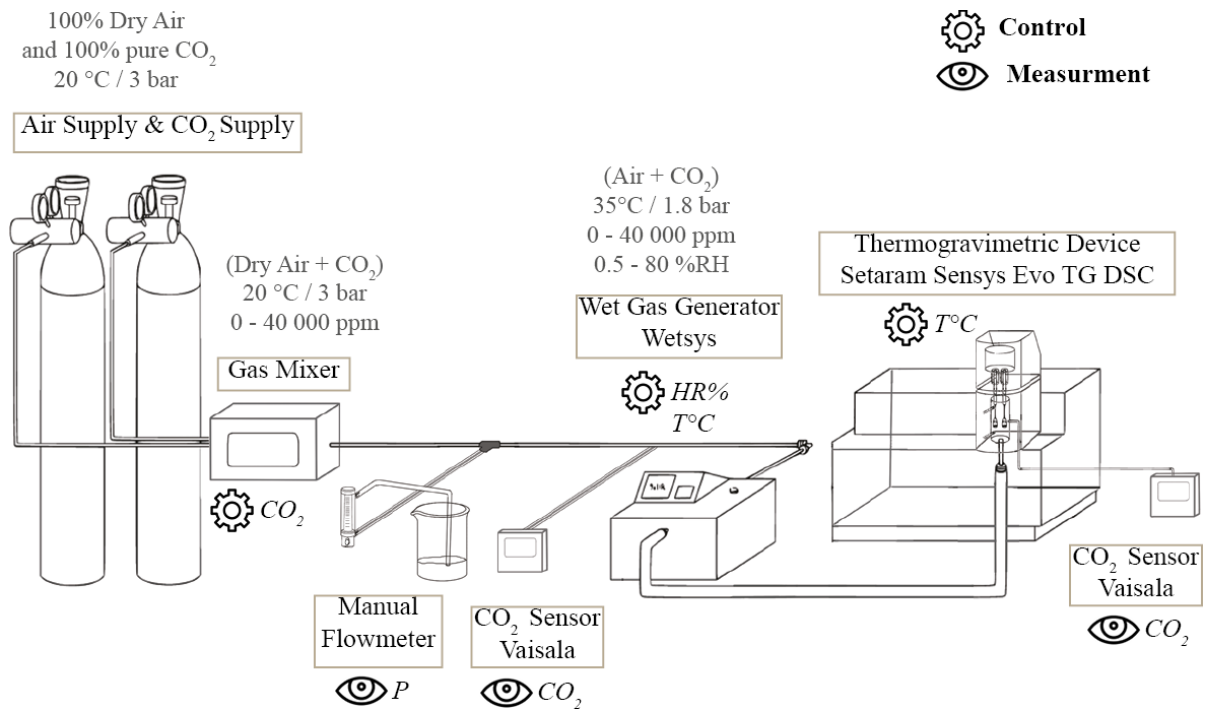


Figure 2: Schematic view of the experimental set-up for carbon dioxide retention measurement

The experimental set up starts with a gas mixer. It was designed using two Burkert<sup>®</sup> Mass Flow Controllers (MFC), one for the CO<sub>2</sub> supply and one for the dry air. It allows a mixture of dry air and CO<sub>2</sub> to be produced by precisely controlling the two flow rates and thus the CO<sub>2</sub> concentration in the mixture. The flow range for the CO<sub>2</sub> MFC is 0 to 0.25 ml/min and the flow range of the dry air MFC is 0 to 0.5 l/min. This system can produce a mixture of air and CO<sub>2</sub> between 0 and 50000 ppm. It is particularly stable in producing low concentrations of CO<sub>2</sub>, around 1500 ppm, representative of those found in indoor air. The desired CO<sub>2</sub> concentration is calculated from the respective flow rates of the two mass flow controllers, which are themselves controlled via the associated Communicator Burkert software. At the outlet of the mixer, a controlled leakage flow generated by a manual flowmeter allows the

136 flow rate to be reduced from 200 ml/min to 50 ml/min for the wet gas generator inlet while maintaining  
137 a sufficient inlet pressure. Part of the gas flow leaves the circuit and ends up in the beaker, allowing  
138 the flow to be reduced without changing the concentration of the mixture. A wet gas generator is then  
139 connected to carry out experiments in a humid environment. Inside the apparatus: the dry inlet gas is  
140 splitted in two lines, one remaining dry and the other one saturated with water. The two gas streams  
141 are mixed in a chamber. To reach the desired relative humidity, the respective flow rates are adjusted  
142 to obtain the required gas mixture. However, as we only consider the dry state in this study, the wetsys  
143 is programmed at 0%RH and only the dry line is opened. The gas is then transferred to the TG-DSC  
144 device with a flow rate of 50 ml/min.

145 The Setaram<sup>®</sup> SENSYS Evo TG-DSC is a thermal analyser used for thermogravimetric (TG) and  
146 differential scanning calorimetry (DSC) measurements. The TG part is composed of a symmetrical  
147 beam balance connected to two columns, one for reference containing either nothing or an inert material,  
148 the other one containing the sample to be measured. The alumina crucibles containing the sample  
149 and the inert material are hung on each side and introduced in the columns. The symmetrical balance  
150 compensates the buoyancy effect, resulting in a very sensitive TG determination. The calorimetry part is  
151 a Tian-Calvet calorimeter which is a heat-flow type with a differential assembly. Heat-flow calorimeters  
152 use several thermocouples connected in serie (e.g. a thermopile) insuring thermal conduction between  
153 the calorimetric cell and its surroundings to measure the heat flow. Here each column (reference and  
154 measure) is surrounded by a thermopile. Heat is measured in all directions. The differential assembly  
155 eliminates the effect of residual thermal disturbances when they arrive in phase on the two thermopiles  
156 connected in opposition. This type of apparatus possesses high sensitivity, which is particularly suitable  
157 for microcalorimetric measurement (energy  $\leq 110$  mJ). In addition, to avoid steam condensation, a  
158 programmable thermostatic bath keeps the oven walls at a temperature above the dew point of the  
159 water vapor. For temperature conditions close to ambient, the experiment cells is regulated with this  
160 thermostatic bath.

161 Finally, a Vaisala<sup>®</sup> CO<sub>2</sub> sensor is used to measure the CO<sub>2</sub> concentration of the gas mixture. Here  
162 it is placed at the outlet of the TG-DSC device.

### 163 **2.3 Test procedure**

164 For this study, it was chosen to work with the driest material possible in order to focus on the interactions  
165 between CO<sub>2</sub> and earth only, without water. The humidity of the experiment is set at 0.5%RH, the lowest  
166 possible value for the wet gas generator. The CO<sub>2</sub> concentration is chosen between 1500 ppm and 10000  
167 ppm. The temperature of the experiment (inlet gas and measuring cell) is set at 35°C, the oven needs

168 a sufficient temperature delta from the ambient to keep the heating power stable. This value may be  
169 considered high for the temperatures encountered in indoor air and knowing that adsorption is favoured  
170 at low temperatures, this choice will have an impact on the adsorbed CO<sub>2</sub>.

171 At the beginning of each experiment, the material is collected in the silica gel box in which it  
172 was stored. Then, the desired sample mass is introduced into the apparatus (usually 110 mg if not  
173 specified). The tests are divided into three stages. The first stage consists of a minimum of three days  
174 of stabilisation, the sample being swept by an air flow without CO<sub>2</sub> at 0.5% RH. Then, successive CO<sub>2</sub>  
175 concentration levels of 5 hours minimum are applied. Finally, to observe the reversibility of the process,  
176 the concentration is reduced to its initial state and applied for a minimum of 5 hours. The duration of  
177 5 hours was chosen on the basis of preliminary studies. During this study, another protocol was also  
178 used, consisting of successive cycles of adsorption at CO<sub>2</sub> concentrations of 5000 ppm and desorption in  
179 between. The tests are carried out in steady state, the measuring cell is considered as an open system  
180 and is continuously swept by the gas mixture. The balance is itself swept by a protective gas (dry air).  
181 Throughout the experiment, the acquisition time is set to 1 point every 2 seconds for the first and third  
182 stage and 1 point every 0.2 seconds for the second stage.

## 183 **3 Results**

### 184 **3.1 Carbon dioxide adsorption and desorption results**

185 Results are presented for a single sample, subjected to eight concentration steps of 12 hours: four steps  
186 of increasing CO<sub>2</sub> concentrations (1500, 3000, 5000, 10000 ppm) and the same steps with decreasing CO<sub>2</sub>  
187 concentrations. The temperature was maintained constant at 35°C. The results will be presented in two  
188 parts: the Thermogravimetry (TG) results and the Differential Scanning Calorimetry (DSC) results.

#### 189 **3.1.1 Thermogravimetry results**

190 The Fig.3 shows the recorded TG signal in  $\mu\text{g}$  and the corresponding CO<sub>2</sub> concentrations in function of  
191 time.

192 For each increase of concentration, a rapid gain in mass is observed, followed by a slower gain until  
193 stabilisation of the mass signal. This mass gain reflects the retention of CO<sub>2</sub> in the material. For each  
194 concentration level, a relatively stable mass is reached after about 10 hours. When the concentration  
195 is decreased, a similar phenomenon is observed: a quasi-instant loss of mass followed by a slower loss  
196 trending towards a stabilisation of the mass. It denotes the release of the retained CO<sub>2</sub>, which would  
197 indicate that all or part of the process is reversible. The reversibility of the process is characteristic of

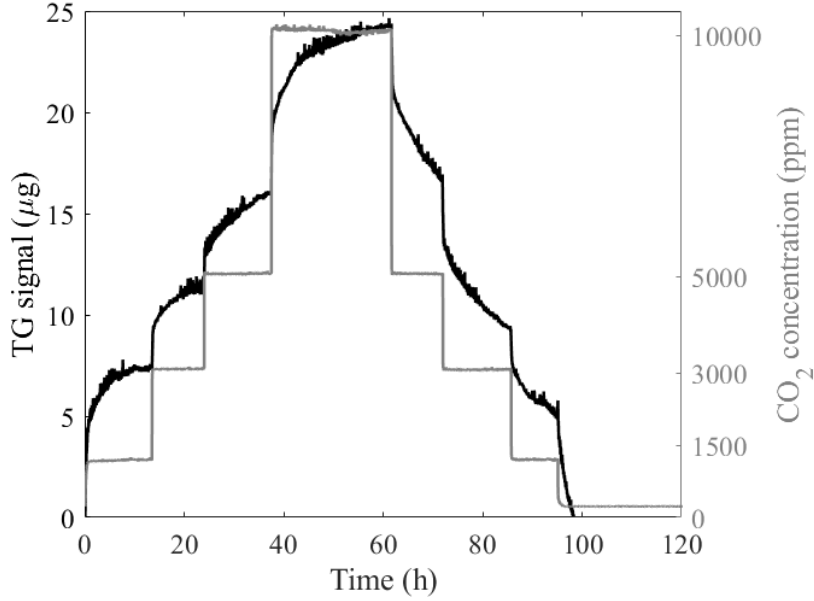


Figure 3: TG signal of the sample exposed to successive levels of CO<sub>2</sub> : 1500, 3000, 5000, 10000 ppm, 35°C and 0.5%RH

198 physisorption: the physical adsorption involving Wan der Waals type interactions. On the opposite, a  
 199 irreversible process would be an indication of chemisorption where chemical reactions are involved [41].  
 200 From these results, the maximum CO<sub>2</sub> retention capacity Q of the material can be calculated for each  
 201 concentration, expressed in mg of adsorbed CO<sub>2</sub> per kg of material. It is calculated from the relative  
 202 mass variation of the sample after and before the concentration step and divided by the initial reference  
 203 sample mass. According to the curves, the results are: 60 mg/kg for 1500 ppm, 97 mg/kg for 3000 ppm  
 204 132 mg/kg for 5000 ppm and 214 mg/kg for 10000 ppm.

### 205 3.1.2 Differential scanning calorimetry results

206 The DSC being a heat flow type the analysed results are heat flows. Results associated to the previous  
 207 experiment are shown in Fig.4. The figure shows the recorded heat flow signal with time and the respec-  
 208 tive carbon dioxide concentration of the gas injected. Upward peaks corresponding to an increase of CO<sub>2</sub>  
 209 concentration are exothermic while downward peaks corresponding to a decrease of CO<sub>2</sub> concentrations  
 210 are endothermic. For the sake of clarity, only a close-up of 2 hours around the change of concentration  
 211 level is represented in order to highlight the beginning of the process.

212 The exothermic peaks associated with a mass gain seem to increase in intensity with higher CO<sub>2</sub>  
 213 concentration. Adsorption is an exothermic process [42], making it thermodynamically favorable which  
 214 is consistent with these results. These heat flows correspond to the physisorption of CO<sub>2</sub> on the surface  
 215 of the material. For each decrement of CO<sub>2</sub> concentration we observe an endothermic peak associated

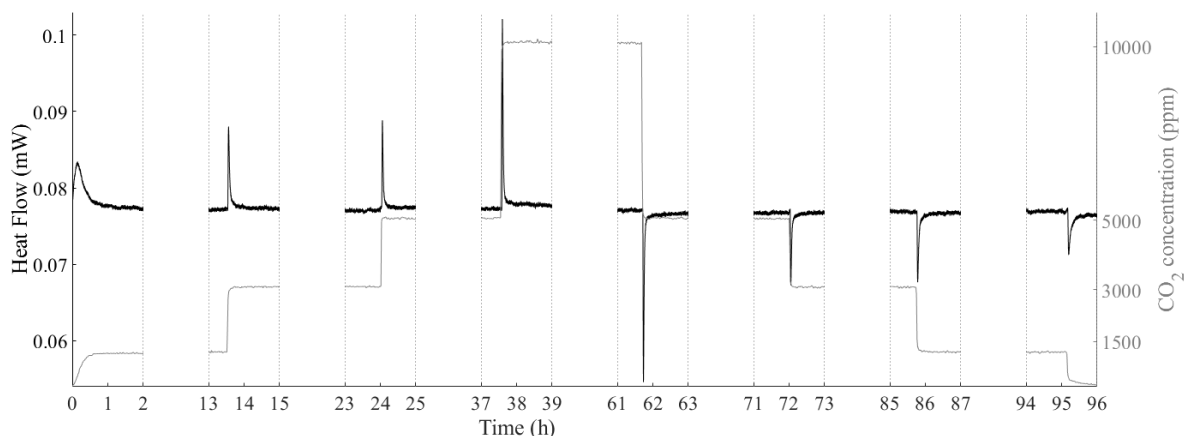


Figure 4: Heat flow signal of the sample exposed to successive levels of CO<sub>2</sub> concentrations: 1500, 3000, 5000, 10000 ppm, at 35°C and 0.5% RH

216 with a mass loss corresponding to a desorption of CO<sub>2</sub>. The response in heat flows is very fast. While the  
 217 mass continues to increase for several hours after the injection of CO<sub>2</sub>, the heat flow variation is hardly  
 218 perceptible after one hour. To go further on that point, the associated enthalpies will be calculated in  
 219 section 4.2.

### 220 3.1.3 Reversibility between adsorption and desorption cycles

221 Previous experiments seem to indicate a reversible physisorption process. In order to confirm this  
 222 hypothesis, a cyclic variation of CO<sub>2</sub> concentration was applied three times, each cycle corresponding  
 223 to 9 hours at 5000 ppm and then 9 hours without CO<sub>2</sub>. The TG results are presented in Fig.5. The  
 224 maximum retention capacity,  $Q$ , is found to be 128 mg/kg for the first cycle, 110 mg/kg and 108 mg/kg  
 225 for the second and the third cycle respectively. Despite a slight decrease, over the 3 cycles, the adsorption  
 226 capacity remains high and we will assume here that this decrease is negligible. Thus, these results tend  
 227 to support the hypothesis that the adsorption is mainly driven by reversible physisorption of CO<sub>2</sub> on  
 228 the clay minerals. However, a clear distinction can not always be made between chemisorption and  
 229 physisorption as intermeditate cases may exist such as adsorption involving strong hydrogen bonds or  
 230 weak charge transfer.

## 231 3.2 Validation of the experimental procedure

### 232 3.2.1 Comparison with a modified Dynamic Vapor Sorption instrument

233 In order to confirm the robustness of the experimental set-up developed with respect to the measured  
 234 mass gains, the thermal analysis was coupled to a DVS (dynamic vapour sorption). It will allow the  
 235 comparison of the mass variations due to CO<sub>2</sub> adsorption/desorption data measured simultaneously on

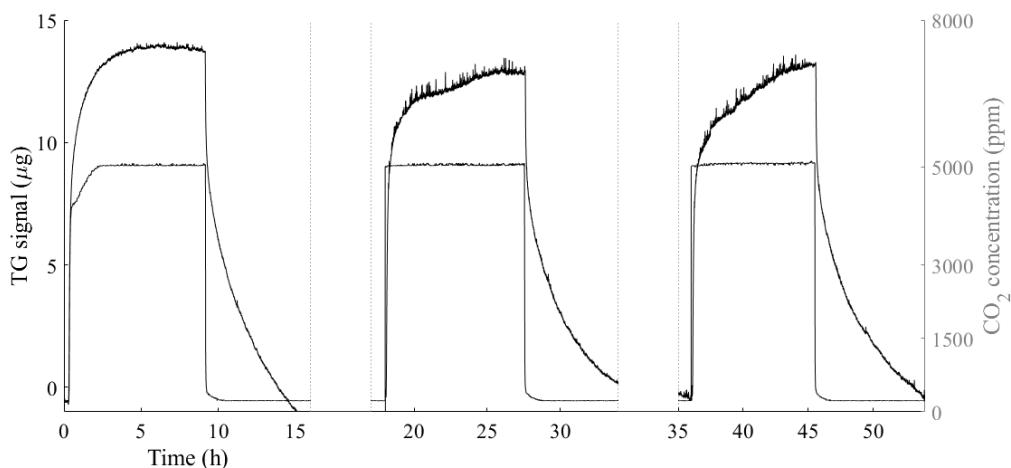


Figure 5: TG signal of the same sample exposed to three CO<sub>2</sub> cycles of (0 - 5000 - 0 ppm) at 35°C and 0.5%RH

236 two different devices. The DVS device, traditionally used to perform water sorption and desorption  
 237 isotherms, consists of a microbalance and a sample holder in the form of a tray allowing larger sample  
 238 masses to be tested which increases the apparent exchange surface (300 mg of sample tested inside the  
 239 DVS compared to 40 mg inside the TG-DSC device here). The coupling was made by connecting the  
 240 outlet of the gas mixer at the inlet of the two apparatus so that two samples of the same earth can be  
 241 tested simultaneously. The humidification phase of the gas is managed separately for the two devices.  
 242 As the minimum in the DVS is 1%RH then it is a limiting factor for the Wetsys, which is then set to  
 243 1%RH and not 0.5%RH as before. The protocol applied was 5 hours of exposition at 5000 ppm and 5  
 244 hours of exposition at 0 ppm. The results are given in Fig.6. The graph shows the relative mass gain in  
 245 mg per kg for the TG-DSC (black) and the DVS (grey) as a function of time. The two samples in the two  
 246 devices appear to behave exactly the same way. It should be noticed that this behaviour appears slightly  
 247 different from the one observed in the previous section. Indeed, there is a rapid gain in mass followed  
 248 by a small loss of mass before reaching equilibrium, which was not present in the previous results. This  
 249 difference can be explained by the presence of water on the adsorption sites, which has an impact on the  
 250 quantity and kinetics of CO<sub>2</sub> adsorption. The mass measurements are similar between the devices and  
 251 confirm the validity of both the TG-DSC device and the use of the DVS device.

### 252 3.2.2 Repeatability of the experiments

253 In order to confront the repeatability of the measurements, the same protocol was repeated on 3 different  
 254 samples of DAG earth with the same initial mass (110mg). The protocol consist of 5 days of stabilisation  
 255 at 0 ppm, 5h of exposition to CO<sub>2</sub> level at 5000 ppm and a return to 0 ppm during 5h. The results are  
 256 shown in Fig.7, the graph a. shows the mass variation versus time of the three tested samples and the

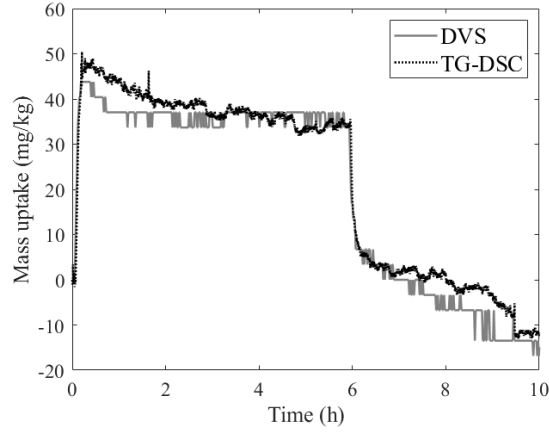


Figure 6: Mass uptake of the samples inside the TG-DSC apparatus (black) and DVS apparatus (grey) when exposed to 5000 ppm, 35°C and 1% RH.

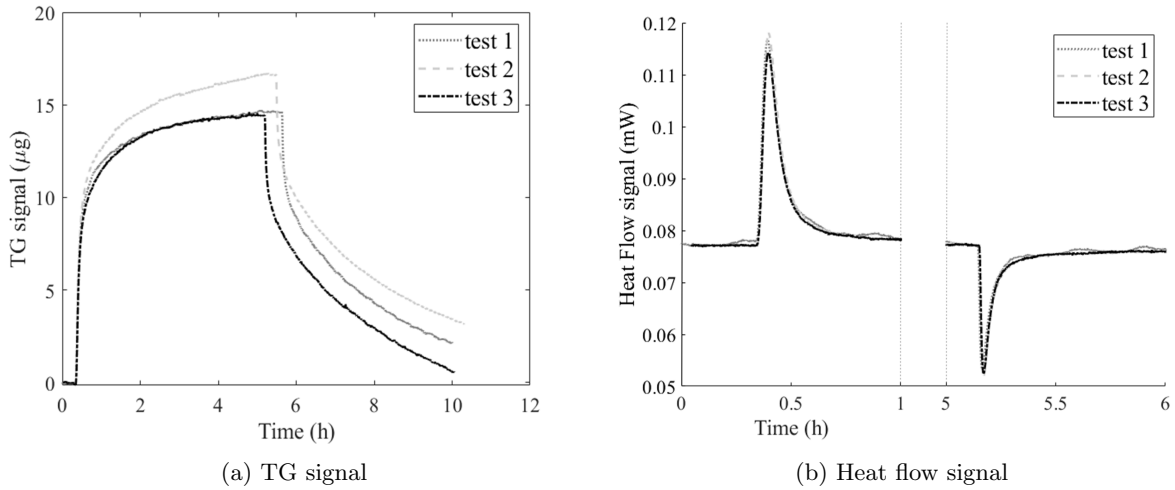


Figure 7: TG (a) and heat flow signals (b) with time of 3 samples exposed to the same conditions (5000 ppm, 35°C and 0.5% RH)

257 graph b. is a 1h zoom on the associated heat flow around the concentration change.

258 The tests were carried out on the 6th of May 2022 (test 1), the 4th of July 2022 (test 2) and the  
 259 26th of August 2022 (test 3) and will be compared with the experiment presented in section 3.1. Fig.7  
 260 highlights a very similar behaviour for the three tests, especially test 1 and test 3 being almost identical.  
 261 The slight difference with test 2 can be explained by the intrinsic variability of the material, as earth is a  
 262 natural material and the composition of this sample may have differed slightly from the other two tests.  
 263 However, the overall behaviour of the sample 2 remains similar in all respects, with a slight increase  
 264 in mass variation, that is reflected in the heat flow. The values of the maximum retention capacity  $Q$   
 265 are: 132 mg/kg for test 1, 146 mg/kg for test 2, 128 mg/kg for test 3, which is similar to the value  
 266 (132 mg/kg) determined for the previous test in the same conditions in section 3.1. From these results  
 267 the mean value of  $Q$  can be calculated as:  $\bar{m} = \frac{1}{n} \sum_{i=1}^n m_i$  with  $m_i$  being the experimental data of the

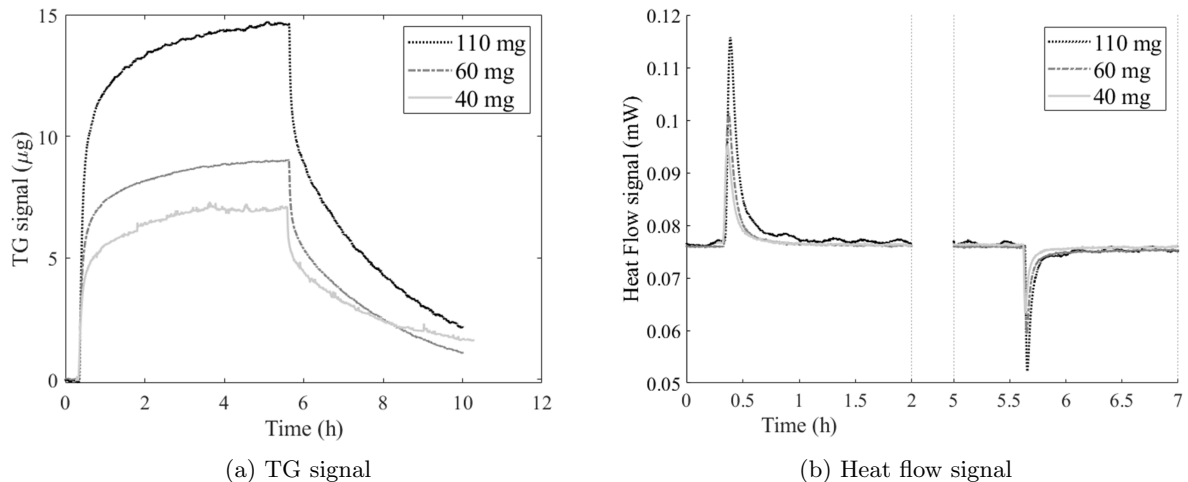


Figure 8: TG (a) and heat flow (a) signals with time of 3 samples with different initial mass exposed to the same conditions (5000 ppm, 35°C and 0.5%RH)

268 four experiments it results in  $\bar{m} = 134$  mg/kg. For the measurement uncertainty, the Student coefficient  
 269 is taken equal to 1.20 corresponding to 4 experiments, the standard deviation can be calculated as:  
 270  $s = \sqrt{\frac{1}{n-1} \sum_{i=1}^n (m_i - \bar{m})^2}$  and results in:  $Q = \bar{m} \pm \frac{st}{\sqrt{n}} = 134 \pm 5$  mg/kg

### 271 3.2.3 Influence of the sample mass

272 The previous experiments were all carried out with 110 mg of material in the crucible of 170  $\mu\text{L}$ , corre-  
 273 sponding to a full crucible. Given the low density of the material in the crucible ( $\rho_d = 0.64\text{g}/\text{cm}^3$ ), the  
 274 hypothesis was made that the  $\text{CO}_2$  diffused perfectly inside the crucible and thus that the whole material  
 275 reacts. In order to confirm this hypothesis experiments were repeated with different initial masses in the  
 276 crucible: 40 mg associated with a nearly empty crucible, 60 mg associated with a slightly more than half  
 277 filling and 110 mg for a full crucible. The results are given in Fig.8.

278 Figure 8 a. presents the TG signal and figure 8 b. the corresponding heat flows (with a 1h-zoom  
 279 around the concentration change) for the three initial masses of material tested. As expected, Fig.8  
 280 shows that the greater the initial mass of the sample is, the greater the mass gain is. This means that  
 281 more  $\text{CO}_2$  is adsorbed when more adsorption sites are available. This indicates that the  $\text{CO}_2$  is diffusing  
 282 within the porous material and that most of the volume of material is active. However, when analysing  
 283 the results in mg of adsorbed  $\text{CO}_2$  per kg of material it can be seen that the maximum adsorption  
 284 capacity seems to increase while there is less sample in the crucible. Indeed, for 110 mg  $Q = 132$  mg/kg,  
 285 for 60 mg  $Q = 142$  mg/kg and for 47 mg  $Q = 155$  mg/kg. This can lead to three hypotheses:

- 286 • Either when the crucible is full, the lower part of the material at the bottom of the crucible does  
 287 not react because the  $\text{CO}_2$  does not diffuse to the bottom.

288 • Or when the crucible is full, drying is not complete in 5 days and water remains in the pores,  
289 blocking adsorption sites that are therefore not available. Whereas when the crucible is not full,  
290 the whole material is dried.

291 • Or we are in the uncertainty range of the measurements and this difference is only a measurement  
292 artefact.

293 Anyway, the difference remains quite small, and it will be assumed to be negligible. Therefore, thanks  
294 to the comparison with the DVS, the methodology for the determination of the mass of CO<sub>2</sub> adsorbed  
295 on DAG was validated. The repetition of the experiments made it possible to calculate the errors in the  
296 uptake capacity measurements and to prove the repeatability. Finally, the robustness to the initial mass  
297 of material was tested. The whole experimental protocol is validated.

## 298 4 Discussion

### 299 4.1 Carbon dioxide adsorption isotherm

#### 300 4.1.1 Carbon dioxide uptake capacity

301 The results of section 3.1 concerning the CO<sub>2</sub> retention capacity  $Q$  in mg/kg and CO<sub>2</sub> concentration in  
302 ppm can be converted into mmol/g and kPa to allow an easier comparison with literature data. This  
303 results in: at 0.12 kPa (1500 ppm) the amount of CO<sub>2</sub> adsorbed is 0.001 mmol/g, at 0.3 kPa (3000  
304 ppm) the amount adsorbed is 0.002 mmol/g, at 0.5 kPa (5000 ppm) it is 0.003 mmol/g and at 1 kPa  
305 (10000 ppm) it is 0.004 mmol/g. The uncertainty calculated before of 5 mg/kg becomes 0.0001 mmol/g.

306 To the best of our knowledge, no study has yet investigated the behaviour of raw earth and clay  
307 minerals with CO<sub>2</sub> at the usual CO<sub>2</sub> pressures of indoor air. The studies we found fall into two categories:  
308 studies on pure clay minerals at high pressure of CO<sub>2</sub> (usually for carbon capture and storage) and studies  
309 on transformed materials at low pressure representative of indoor air.

310 As expected, the results found here are much lower than those of the first group of papers, mainly  
311 because our material is less pure (only 19% of clay minerals in DAG) and the pressures investigated  
312 are lower. For example, Chen et al. [43] [44] mentioned an adsorption capacity for raw kaolinite at  
313 25°C and 1 bar between 0 and 0.07 mmol/g. Several authors also reported adsorption capacities for  
314 montmorillonite between 0.2 mmol/g at 45°C and 1 bar and 0.5 mmol/g at 10°C and 1 bar [45] [46].  
315 Although the test temperatures are different and known to affect adsorption, the range of variation can  
316 be considered small and does not affect the order of magnitude of the adsorption results. The trend  
317 should remain the same. The impact of temperature should be assessed to confirm this statement.

318 Our results are also lower than those found in the second group of papers. These studies mainly  
319 focus on materials transformed in laboratories such as zeolites, metal-organic frameworks (MOF) or  
320 activated carbons. The table 2 gathers the main results obtained. The highest adsorption capacities (2.8  
321 mmol/g for a MOF at 60%RH and 1000 ppm [22]) are found to be associated with materials with low  
322 regenerability (e.g the capacity to release the CO<sub>2</sub> retained at ambient condition of temperature and  
323 humidity). Rajan et al. [20] reported adsorption capacities ranging from 1.42 to 1.62 mmol/g at 0% RH  
324 and 3000 ppm for MOF, zeolite and silica-supported amine (PD-TEPA) powders, but their regeneration  
325 capacity was very low (30 % for the amines) or even nul for zeolite and MOF. According to the literature,  
326 it seems that some amines have a good regeneration capacity as analysed by Krishnamurthy et al. [21],  
327 but the cost as well as the stability of these materials to hygrothermal conditions of indoor air may be  
328 a limiting factor to their wide use as wall coating.

329 Thus, the adsorption capacity of DAG earth at different CO<sub>2</sub> concentrations is much lower than the  
330 capacities of other materials reported in the literature. It should be kept in mind that the material  
331 studied is a natural and unprocessed material and that it can be applied in large quantities on the wall  
332 and ceiling surfaces of a room, which would compensate for its relatively low adsorption capacity. For  
333 example, plasters made from the same earth in previous studies ([35] [36]) had an apparent density  
334 between 1.5 and 1.9  $g/cm^3$  for a formulation containing 40% earth sieved at 2 mm. Reducing this  
335 percentage to the fraction studied here ( $< 80\mu m$ ) and for a plaster thickness of 1 cm would give between  
336 5 and 7  $kg/m^2$  of our material per square meter of wall.

Table 2: Confrontation between DAG CO<sub>2</sub> uptake capacity and those reported in the literature for porous materials at room temperature

Material		CO <sub>2</sub> uptake [mmol/g]	Desorption capacity [%]	Exp. conditions [%RH, ppm]	Ref.
DAG	powder	0.003	100	0.5, 5000	This study
Latex+TEPA70 <sup>a</sup>	powder	1.33	92	15, 3000	[21]
	paint	1			
Latex+PEI50 <sup>b</sup>	powder	1.1			
	paint	0.8			
epn-MOF@SBS <sup>c</sup>	spray	2.8	0	60, 1000	[22]
PD-TEPA-25% <sup>d</sup>	powder	1.36	30	0, 3000	[20]
MOF-74(Mg) <sup>e</sup>		1.62	0		
Zeolite-13X		1.42	0		

<sup>a</sup> Silica including amine (TEPA), 40 wt%    <sup>b</sup> Silica including amine (PEI) 40 wt%

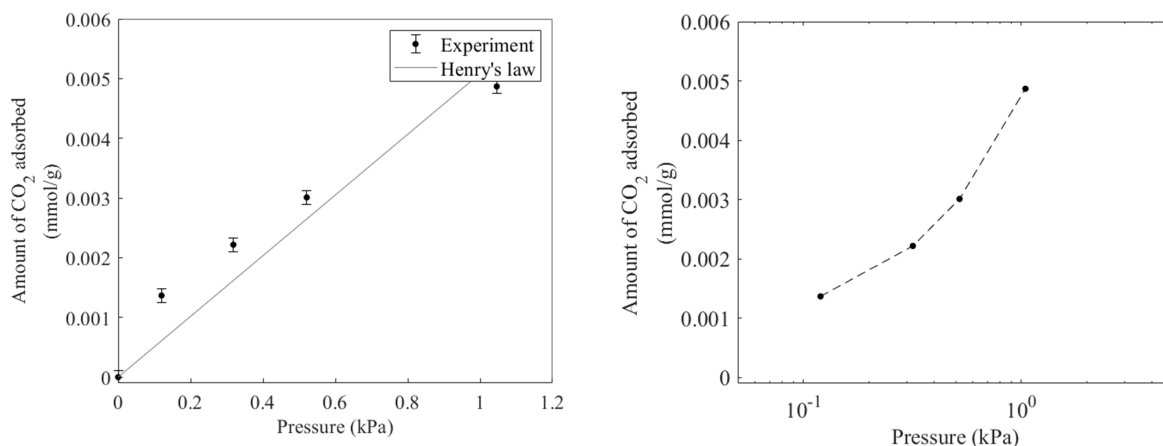
<sup>c</sup> Functionalized metal-organic-framework mixing with a hydrophobic polymer (SBS), 80 wt% MOF loading

<sup>d</sup> Silica including amines (TEPA) 25%wt    <sup>e</sup> Metal-organic framework

#### 338 4.1.2 Modelling the adsorption isotherm using Henry's law

339 As the experiments were carried out at low pressure (less than 1.2 kPa), the isotherm of CO<sub>2</sub> adsorption  
 340 on DAG can be analysed using Henry's law. This empirical law translates the fact that at low pressure  
 341 the adsorbed molecules are independent of each other. It can be expressed as:  $n = k_h p$ . Where  $n$   
 342 represents the specific surface excess amount and  $k_h$  the Henry's law constant. Thus, at sufficiently low  
 343 pressures,  $n$  should vary linearly with the equilibrium gas pressure. It was originally defined to study  
 344 the amount of gas dissolved in a liquid, but it reflects the general principle that can be applied to gas  
 345 adsorption: when the adsorbate concentration tends to 0, the amount adsorbed also tends to 0.

346 In figure 9a there is the fitting of the experimental data with Henry's law, the results give a constant  
 347 of 0.005 mmol/(g\*kPa) with an  $R^2$  of 0.90. This value is very low compared to those reported for other  
 348 adsorbents such as: modified zeolites [47] or pillared clays [48] which are in the range of 0.012 to 0.05  
 349 at 293 K and 310 K respectively. These results are in line with the values obtained for CO<sub>2</sub> uptake, i.e.  
 350 much lower compared to chemically modified materials. Even though the experiments are carried out  
 351 at very low pressures where Henry's law should apply, from the figure it seems that the fitting is not  
 352 very consistent. As stated in Rouquerol et al. [49], the hypothesis needed for the application of Henry's



(a) CO<sub>2</sub> adsorption isotherm and associate Henry's law fit

(b) CO<sub>2</sub> adsorption isotherm in semi-log scale

Figure 9: Modelling of the adsorption isotherm using the Henry's law (a) and evidence of non-consistent fitting by plotting the adsorption isotherm in semi-log scale (b)

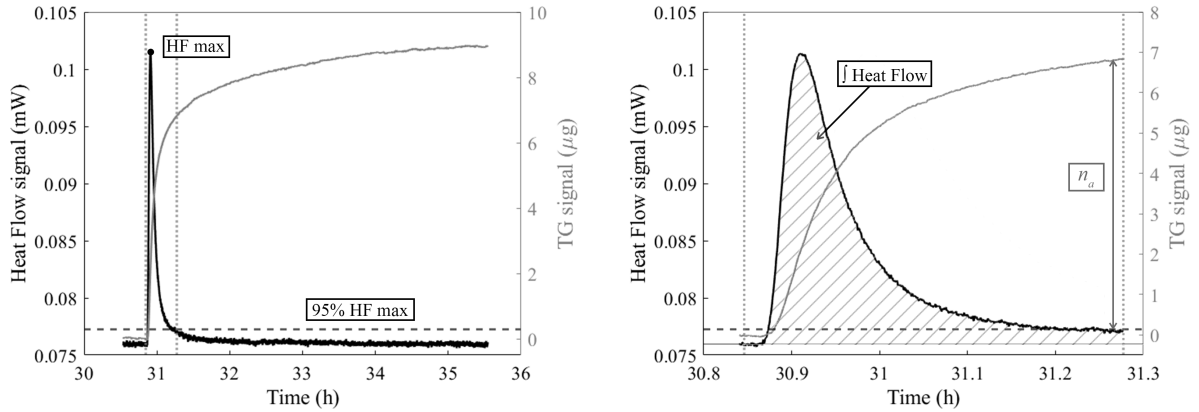
353 law can be easily verified by plotting the isotherm on a semi-logarithmic scale. In figure 9b one can see  
 354 the isotherm plotted on a semi-logarithmic scale. It appears clearly that the plot is not linear. At the  
 355 beginning of the curve, a convex deviation could be attributed to the effect of either surface heterogeneity  
 356 or microporosity in the interlayer space of clay minerals. Indeed, some specific adsorbent-adsorbate  
 357 interactions can be associated with energetic heterogeneity. This case was identified by Rouquerol et al.  
 358 [49] and the adsorption energies should help to establish whether this bend is associated with adsorption  
 359 on a small high-energy fraction of the surface or whether adsorbate-adsorbate interactions are detectable  
 360 over the linear range. Anyway, this indicates the need for another form of approximation for the isotherm  
 361 at low concentrations.

362 Thus, modelling the adsorption isotherm with Henry's law has shown the existence of non-linear  
 363 phenomena at low pressures. These phenomena can be explained either by the entry of CO<sub>2</sub> into the  
 364 micropores of clay minerals (interlayer space for example) or by CO<sub>2</sub>-CO<sub>2</sub> interactions or by a strong  
 365 surface heterogeneity (presence of adsorption sites with more energy than others).

## 366 4.2 Adsorption and desorption enthalpies

### 367 4.2.1 Methodology for the determination of CO<sub>2</sub> adsorption enthalpy

368 Thermodynamically, enthalpy of adsorption (or desorption) is the heat released (or absorbed) during the  
 369 adsorption process. The enthalpy of adsorption,  $\Delta h_{ads}$ , was determined by calculating the area under  
 370 the heat flow signal curve and dividing by the associated mass change during the adsorption phase. The  
 371 same process was applied on the desorption phase to determine the desorption enthalpy. The baseline  
 372 for the signal integration was chosen as the median of the points preceding the peak. In order to get rid



(a) Full heat flow signal for a given  $\text{CO}_2$  concentration (b) Extracted heat flow signal between the limits of integration for a given  $\text{CO}_2$  concentration

Figure 10: Limits of integration (vertical dotted lines) to determine  $\text{CO}_2$  adsorption enthalpy from TG and DSC signals

373 of the background noise of the signal during integration, the choice was made to narrow the integration  
 374 boundaries as much as possible while keeping the major part of the signal, this procedure is detailed in  
 375 fig.10. To do this, the maximum value of HF was calculated (10a: "HF max"). Then, 95% of this value  
 376 was subtracted from the peak to reach the line "95% HF max" (10a: "95% HF max"). The intersection  
 377 between this line and the HF curve determined the upper and lower boundaries for the integration.  
 378 Finally, a time interval was subtracted to the lower boundary to include the beginning of the heat flow  
 379 peak in the calculations. The signal obtained between the two boundaries corresponds to figure 10b.  
 380 In other words, integration was performed between the beginning of the peak and 95% of its maximum  
 381 value. The integration result (10b: " $\int \text{HeatFlow}$ ") was then divided by the corresponding mass uptake  
 382 (10b: " $n_a$ "). The same procedure was applied for the determination of the enthalpy of desorption.

383 The enthalpies have been calculated for all experiments conducted between 0 and 5000 ppm and are  
 384 given in Table 3. The enthalpy of adsorption is negative because the flow is exothermic and the enthalpy  
 385 of desorption is positive as associated with an endothermic flow. Results indicate that  $\Delta h_{ads}$  is found to  
 386 be equal to approx. -60 kJ/kg and  $\Delta h_{des}$  to approx. 55 kJ/mol for all experiments. The experiments are  
 387 therefore perfectly repeatable in terms of energy. It can be noticed that the initial mass of the sample has  
 388 little influence on the final adsorption and desorption enthalpy result. For the adsorption and desorption  
 389 cycles,  $\Delta h_{ads}$  decreases when the number of cycles increases which is in agreement with the results found  
 390 for the  $\text{CO}_2$  uptake capacity and has to be further investigated. In general, the results of adsorption  
 391 enthalpies found are quite high for physisorption which is generally around 20 to 40 kJ/mol which would  
 392 indicate a strong energetic interaction between the adsorption sites and the  $\text{CO}_2$ . Enthalpies above  
 393 40 kJ/mol could indicate chemisorption, but the reversibility of the process, when the concentration  
 394 decreases, seems to rule out this hypothesis. Moreover, chemisorption enthalpies found in the literature

395 for clay minerals are generally above 80 kJ/mol, which is far from being the case here [50].

396

Table 3: Enthalpies of adsorption and desorption of all experiments at 0.5% RH, 35°C 5000 ppm

<b>Experiment</b>	$\Delta h_{ads}$	$\Delta h_{des}$	<b>Section</b>
	[kJ/mol]	[kJ/mol]	
Test 1	-62	56	sec.3.2.2
Test 2	-60	60	sec.3.2.2
Test 3	-61	56	sec.3.2.2
110 mg	-62	56	sec.3.1.1
63 mg	-60	57	sec.3.2.3
47 mg	-56	55	sec.3.2.3
Cycle 1	-61	56	sec.3.1.3
Cycle 2	-58	57	sec.3.1.3
Cycle 3	-54	56	sec.3.1.3

397 To our knowledge, no study has yet published data on the enthalpy of CO<sub>2</sub> adsorption in raw earth  
398 or clay minerals. Hence, the results of this study are compared with those of processed materials (MOF,  
399 amines..) used for CO<sub>2</sub> regulation of indoor air, in the same way as in previous sections (see table  
400 4). Two methods are mainly used to determine the enthalpy of adsorption of CO<sub>2</sub> on materials, the  
401 "indirect" isosteric method based on CO<sub>2</sub> adsorption and desorption isotherms at several temperatures  
402 and the calorimetric method (used here). The calorimetric method is the more accurate method as it  
403 provides a direct measurement. For silica-supported amines [51], pillard clays [48] and zeolites [52] values  
404 of the enthalpy of CO<sub>2</sub> adsorption are ranging from -90 to -30 kJ/mol at low coverage (i.e. low surface  
405 occupancy, low amount adsorbed). Similarly, Wu et al. [53] has determined the enthalpy of adsorption at  
406 25°C by calorimetric measurement of a MOF, at zero-coverage an irreversible event of -113 kJ/mol occurs  
407 which is followed by a reversible event of -65 kJ/mol and finally a plateau at -40 kJ/mol is observed  
408 as coverage is increased. Our results, around -60 kJ/mol at adsorption, are thus in the range of values  
409 found in other studies. This confirms both the robustness of the experimental set-up with respect to  
410 the analysis of heat flow and the determination of CO<sub>2</sub> adsorption enthalpies. It also reinforces the  
411 hypothesis that the phenomena are mainly driven by physical interactions.

Table 4: Comparison of the CO<sub>2</sub> adsorption enthalpy of DAG with those reported in the literature for porous material at low adsorption site occupancy

Material	Exp. conditions (method)	$\Delta H_{ads}$ [kJ/mol]	Ref.
DAG 80 $\mu$ m	0.5%RH 35°C (calorimetric)	-60	This study
SBA 15+ APS <sup>a</sup>	30°C (calorimetric)	[-40,-90]	[51]
Al-, Zr-PILC <sup>b</sup>	[-10, 20]°C (isosteric)	-30	[48]
Zeolite 13X	0°C (calorimetric)	-55	[52]
CD-MOF-2 <sup>c</sup>	25°C (calorimetric)	-113.5 (irreversible)	[53]
		-65.4 (reversible)	
		-40.1 (reversible)	

<sup>a</sup> Mesoporous silica (SBA-15) support with amine (APS) loadings    <sup>b</sup> Pillared clays

<sup>c</sup> Metal-organic framework synthesized from  $\gamma$  cyclodextrin ( $\gamma$ -CD)

#### 4.2.2 Impact of the adsorbed quantity on the enthalpy

In order to follow the evolution of the enthalpy as a function of the amount of CO<sub>2</sub> adsorbed, the calculation of the adsorption and desorption enthalpies were repeated between the successive CO<sub>2</sub> concentration steps of the experiment in section 3.1 ( 1500, 3000, 5000 and 10000 ppm). The results are given in Figure 11, the differential enthalpy of adsorption (left) or desorption (right) between two states was calculated for the successive CO<sub>2</sub> steps.

The covering can be defined as the surface occupation by the CO<sub>2</sub> molecules. It increases with the amount adsorbed. From the graph it can be seen that  $\Delta h_{ads}$  is higher for the first range of concentrations and progressively decreases towards -40 kJ/mol as the coverage increases. Theoretically, if the concentration of CO<sub>2</sub> continues to increase, the values of adsorption enthalpy should tend towards the enthalpy of vaporisation of CO<sub>2</sub> (-17 kJ/mol at 288 K), but this comparison is difficult to make at 35°C because the triple point of CO<sub>2</sub> has passed and no change of state between the gas and liquid phase can take place. In all cases, the first values of -74 kJ/mol are very high and the last values of about -40 kJ/mol are in agreement with the values found in the literature for physisorption. The high initial values can be associated with the interaction of adsorptive molecules with highly active surface sites and/or their entry into narrow micro-pores. The reason that the enthalpy of adsorption decreased with increasing coverage is due to the progressive covering of the thermodynamically favorable sites, such that the most favorable sites are filled first, followed by the remaining sites. Going back to the Henry's law analysis, it can be

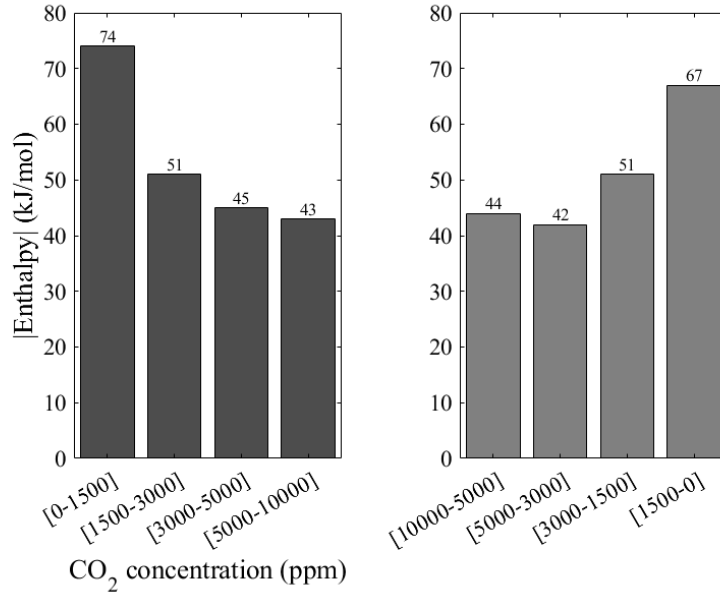


Figure 11: Absolute values of enthalpies of adsorption (black) and desorption (gray) for successive CO<sub>2</sub> concentration levels, at 0.5% RH and 35°C

431 deduced that the knee found at low pressures is more likely to represent a strong energy heterogeneity  
 432 than interactions between CO<sub>2</sub> molecules (adsorbate-adsorbate) which would have been represented by  
 433 an increase of enthalpy with covering.

434 All the analyses carried out in the discussion section show that the phenomenon is dominated by  
 435 physical interactions (even if a sharp distinction is not possible and desired because intermediate cases  
 436 exist). Secondly, at low pressures, the heterogeneity of the material surface leads to the adsorption of the  
 437 first CO<sub>2</sub> molecules on very energetic sites (or micropore), followed by the adsorption on less energetic  
 438 sites.

## 439 5 Conclusions and perspectives

440 The aim of this paper was to present a new experimental methodology based on thermogravimetry  
 441 coupled with calorimetric analysis to evaluate the CO<sub>2</sub> retention capacities of raw earth. The coupling  
 442 of the TG-DSC apparatus was done with a gas mixer capable of producing an air flow with low CO<sub>2</sub>  
 443 concentration representative of indoor air and with a wet gas generator to represent several relative  
 444 humidity. For the dry state: the set-up and experimental procedure were validated through repeatability  
 445 testing and coupling to a DVS, while the robustness of the device was demonstrated with respect to  
 446 the initial masses of materials tested. Considering the results obtained, at 5000 ppm the dry raw  
 447 earth material has a maximum CO<sub>2</sub> retention capacity of about 134 mg/kg and an almost complete

448 regeneration capacity at 35°C. The almost complete reversibility of the process shows that the CO<sub>2</sub> is  
449 physisorbed, most likely on the surface of the clay minerals present in the material. The determination  
450 of the enthalpies of adsorption allowed to characterize precisely the processes involved. At 5000 ppm the  
451 enthalpy of adsorption is -60 kJ/mol and the one of desorption is 55 kJ/mol on average, the value we  
452 found is higher than the enthalpies associated with physisorption which are between 20 and 40 kJ/mol.  
453 However, when the enthalpies were examined as a function of the quantity adsorbed, it was found that  
454  $\Delta h_{ads}$  varied from -70 kJ/mol to -40 kJ/mol when the quantity adsorbed was increased. This indicates  
455 the presence of a strong energetic heterogeneity of the material or the entry of CO<sub>2</sub> in micropores, which  
456 is confirmed by the non-linearity of the isotherm at low pressures. These results are in agreement with  
457 the fact that raw earth is a natural and highly heterogeneous material.

458 As indoor air also contains water vapour, it is crucial to determine the role of water in the CO<sub>2</sub>  
459 retention and release process. Research is underway to analyse the phenomena at higher relative  
460 humidity (between 50%RH and 80%RH) in order to understand the possible competition between the  
461 water and CO<sub>2</sub> molecules adsorbed. This work provides the first values of CO<sub>2</sub> retention capacity for  
462 raw earth and thus provides first evidence of the potential passive regulation capacity of this material. A  
463 better understanding of the mechanisms will allow us to better understand the benefits of raw earth for  
464 using it in a passive strategy to improve IAQ and can therefore lead to its wider uses by the construction  
465 and building sector.

## 466 Acknowledgments

467 This project has received funding from the European Union’s Horizon 2020 research and innovation  
468 program under the Marie Skłodowska-Curie grant agreement No 945416, the Institut Universitaire de  
469 France, the IMPULSION PALSE program, the CARNOT institute and the Chair ConstrucTerr.

## 470 References

- 471 [1] Mohamad Awada, Burçin Becerik-Gerber, Elizabeth White, Simi Hoque, Zheng O’Neill, Giulia  
472 Pedrielli, Jin Wen, and Teresa Wu. Occupant health in buildings: Impact of the COVID-19 pandemic  
473 on the opinions of building professionals and implications on research. *Building and Environment*,  
474 207:108440, January 2022.
- 475 [2] M.Y.Z. Abouleish. Indoor air quality and COVID-19. *Public Health*, 191:1–2, February 2021.
- 476 [3] A. P. Jones. Indoor air quality and health. *Atmospheric Environment*, 33(28):4535–4564, December  
477 1999.

- 478 [4] United Nations Environment Programme. 2020 Global Status Report for Buildings and Construc-  
479 tion: Towards a Zero-emission, Efficient and Resilient Buildings and Construction Sector. Global  
480 Status Report for Buildings and Construction, UNEP, Nairobi, 2020.
- 481 [5] Luis Pérez-Lombard, José Ortiz, and Christine Pout. A review on buildings energy consumption  
482 information. *Energy and Buildings*, 40(3):394–398, January 2008.
- 483 [6] Séverine Kirchner, Jean-François Arenes, Christian Cochet, Mickael Derbez, Cédric Duboudin,  
484 Patrick Elias, Anthony Gregoire, Béatrice Jédor, Jean-Paul Lucas, Nathalie Pasquier, Michèle  
485 Pigneret, and Olivier Ramalho. État de la qualité de l’air dans les logements français. *Envi-  
486 ronnement, Risques & Santé*, 6(4):259–269, July 2007.
- 487 [7] Neil E. Klepeis, William C. Nelson, Wayne R. Ott, John P. Robinson, Andy M. Tsang, Paul Switzer,  
488 Joseph V. Behar, Stephen C. Hern, and William H. Engelmann. The National Human Activity  
489 Pattern Survey (NHAPS): a resource for assessing exposure to environmental pollutants. *Journal of  
490 Exposure Science & Environmental Epidemiology*, 11(3):231–252, July 2001. Number: 3 Publisher:  
491 Nature Publishing Group.
- 492 [8] Sotiris Vardoulakis, Chrysanthi Dimitroulopoulou, John Thornes, Ka-Man Lai, Jonathon Taylor,  
493 Isabella Myers, Clare Heaviside, Anna Mavrogianni, Clive Shrubsole, Zaid Chalabi, Michael Davies,  
494 and Paul Wilkinson. Impact of climate change on the domestic indoor environment and associated  
495 health risks in the UK. *Environment International*, 85:299–313, December 2015.
- 496 [9] Tyler A. Jacobson, Jasdeep S. Kler, Michael T. Hernke, Rudolf K. Braun, Keith C. Meyer, and  
497 William E. Funk. Direct human health risks of increased atmospheric carbon dioxide. *Nature  
498 Sustainability*, 2(8):691–701, August 2019.
- 499 [10] Kenichi Azuma, Naoki Kagi, U. Yanagi, and Haruki Osawa. Effects of low-level inhalation expo-  
500 sure to carbon dioxide in indoor environments: A short review on human health and psychomotor  
501 performance. *Environment International*, 121:51–56, December 2018.
- 502 [11] Jie Zhang, Xiaodong Cao, Xin Wang, Liping Pang, Jin Liang, and Liang Zhang. Physiological  
503 responses to elevated carbon dioxide concentration and mental workload during performing MATB  
504 tasks. *Building and Environment*, 195:107752, May 2021.
- 505 [12] Jie Zhang, Liping Pang, Xiaodong Cao, Xiaoru Wanyan, Xin Wang, Jin Liang, and Liang Zhang.  
506 The effects of elevated carbon dioxide concentration and mental workload on task performance in  
507 an enclosed environmental chamber. *Building and Environment*, 178:106938, July 2020.

- 508 [13] ASHRAE. ANSI/ASHRAE Standard 62.1-2013: The standards For Ventilation And Indoor Air  
509 Quality. Technical report, American Society for Heating, Refrigeration and Air Conditioning Engi-  
510 neering, Atlanta, 2013.
- 511 [14] European Commission. Joint Research Centre. Institute for Health and Consumer Protection., Eu-  
512 ropean Commission. Directorate General for Health and Consumers., and Regional Environmental  
513 Centre for Central and Eastern Europe. *SINPHONIE: Schools Indoor Pollution & Health Observa-*  
514 *tory Network in Europe : final report*. Publications Office, LU, 2014.
- 515 [15] Máté Szabados, Réka Kakucs, Anna Páldy, Bohumil Kotlík, Helena Kazmarová, Arianna Dongio-  
516 vanni, Andrea Di Maggio, Anna Kozajda, Anja Jutraz, Andreja Kukec, Peter Otorepec, and Tamás  
517 Szigeti. Association of parent-reported health symptoms with indoor air quality in primary school  
518 buildings – The InAirQ study. *Building and Environment*, 221:109339, August 2022.
- 519 [16] Zahra Shayegan, Mitra Bahri, and Fariborz Haghighat. A review on an emerging solution to improve  
520 indoor air quality: Application of passive removal materials. *Building and Environment*, 219:109228,  
521 July 2022.
- 522 [17] Teresa M. Mata, António A. Martins, Cristina S. C. Calheiros, Florentina Villanueva, Nuria P.  
523 Alonso-Cuevilla, Marta Fonseca Gabriel, and Gabriela Ventura Silva. Indoor Air Quality: A Review  
524 of Cleaning Technologies. *Environments*, 9(9):118, September 2022.
- 525 [18] Victor Gold, editor. *The IUPAC Compendium of Chemical Terminology: The Gold Book*. Inter-  
526 national Union of Pure and Applied Chemistry (IUPAC), Research Triangle Park, NC, 4 edition,  
527 2019.
- 528 [19] Elliott T. Gall and William W Nazaroff. New directions: Potential climate and productivity benefits  
529 from CO<sub>2</sub> capture in commercial buildings. *Atmospheric Environment*, 103:378–380, February 2015.
- 530 [20] P. E. Rajan, A. Krishnamurthy, G. Morrison, and F. Rezaei. Advanced buffer materials for indoor  
531 air CO<sub>2</sub> control in commercial buildings. *Indoor Air*, 27(6):1213–1223, November 2017.
- 532 [21] Anirudh Krishnamurthy, Buddhabhushan Salunkhe, Ashish Zore, Ali Rownaghi, Thomas Schuman,  
533 and Fateme Rezaei. Amine-Based Latex Coatings for Indoor Air CO<sub>2</sub> Control in Commercial  
534 Buildings. *ACS Applied Materials & Interfaces*, 11(18):16594–16604, May 2019.
- 535 [22] Yun Seok Chae, Sookyung Park, Dong Won Kang, Dae Won Kim, Minjung Kang, Doo San Choi,  
536 Jong Hyeak Choe, and Chang Seop Hong. Moisture-tolerant diamine-appended metal–organic frame-  
537 work composites for effective indoor CO<sub>2</sub> capture through facile spray coating. *Chemical Engineering*  
538 *Journal*, 433:133856, April 2022.

- 539 [23] Shih Ching Lee, Chu Chin Hsieh, Chien Hung Chen, and You Syuan Chen. CO<sub>2</sub> Adsorption  
540 by Y-Type Zeolite Impregnated with Amines in Indoor Air. *Aerosol and Air Quality Research*,  
541 13(1):360–366, 2013.
- 542 [24] Minjae Kim, Jae Won Lee, Seonggon Kim, and Yong Tae Kang. CO<sub>2</sub> adsorption on zeolite 13X  
543 modified with hydrophobic octadecyltrimethoxysilane for indoor application. *Journal of Cleaner*  
544 *Production*, 337:130597, February 2022.
- 545 [25] Shuang Wang, Yu-Ri Lee, Yooseob Won, Hana Kim, Se-Eun Jeong, Byung Wook Hwang, A. Ra Cho,  
546 Jae-Young Kim, Young Cheol Park, Hyungseok Nam, Dong-Ho Lee, Hyunuk Kim, and Sung-Ho  
547 Jo. Development of high-performance adsorbent using KOH-impregnated rice husk-based activated  
548 carbon for indoor CO<sub>2</sub> adsorption. *Chemical Engineering Journal*, 437:135378, June 2022.
- 549 [26] Fionn McGregor, Andrew Heath, Andrew Shea, and Mike Lawrence. The moisture buffering capacity  
550 of unfired clay masonry. *Building and Environment*, 82:599–607, December 2014.
- 551 [27] Monika Woloszyn, Targo Kalamees, Marc Olivier Abadie, Marijke Steeman, and Angela Sasic Kala-  
552 gasidis. The effect of combining a relative-humidity-sensitive ventilation system with the moisture-  
553 buffering capacity of materials on indoor climate and energy efficiency of buildings. *Building and*  
554 *Environment*, 44(3):515–524, March 2009.
- 555 [28] Jean-Claude Morel, Rabia Charef, Erwan Hamard, Antonin Fabbri, Chris Beckett, and Quoc-Bao  
556 Bui. Earth as construction material in the circular economy context: practitioner perspectives  
557 on barriers to overcome. *Philosophical Transactions of the Royal Society B: Biological Sciences*,  
558 376(1834):20200182, September 2021. Publisher: Royal Society.
- 559 [29] E. Darling and R. L. Corsi. Field-to-laboratory analysis of clay wall coatings as passive removal  
560 materials for ozone in buildings. *Indoor Air*, 27(3):658–669, May 2017.
- 561 [30] Erin K. Darling, Clement J. Cros, Pawel Wargocki, Jakub Kolarik, Glenn C. Morrison, and  
562 Richard L. Corsi. Impacts of a clay plaster on indoor air quality assessed using chemical and  
563 sensory measurements. *Building and Environment*, 57:370–376, November 2012.
- 564 [31] S Roucan, F McGregor, A Fabbri, C Perlot-Bascoulès, and J-C Morel. Indoor CO<sub>2</sub> buffering po-  
565 tential of clay-based building materials. *IOP Conference Series: Earth and Environmental Science*,  
566 1078(1):012135, September 2022.
- 567 [32] Maria Gomes and Teresa Miranda. Indoor air quality for sustainability, occupational health and  
568 classroom environments through the application of earth plaster. In *Proceedings HERITAGE 2022*

- 569 - *International Conference on Vernacular Heritage: Culture, People and Sustainability*, pages  
570 363–368. Editorial Universitat Politècnica de València, September 2022. Accepted: 2022-10-  
571 31T10:09:05Z.
- 572 [33] T. Santos, P. Faria, and M. I. Gomes. Earth, Gypsum and Cement-Based Plasters Contribution to  
573 Indoor Comfort and Health. In Eduardo B. Pereira, Joaquim A. O. Barros, and Fabio P. Figueiredo,  
574 editors, *Proceedings of the 3rd RILEM Spring Convention and Conference (RSCC2020)*, RILEM  
575 Bookseries, pages 105–117, Cham, 2021. Springer International Publishing.
- 576 [34] Noha Al Haffar. *Efficient stabilization with hydraulic binders of local earth for building construction*  
577 *applications*. Theses, Université de Lyon, June 2021. Issue: 2021LYSET006.
- 578 [35] T. Mauffré, E. Keita, E. Contraires, F. McGregor, and A. Fabbri. Analysis of water droplet pen-  
579 etration in earth plasters using X-ray microtomography. *Construction and Building Materials*,  
580 283:122651, May 2021.
- 581 [36] F. McGregor, T. Mauffré, M.-S. Force, E. Contraires, and A. Fabbri. Measurement of the water  
582 vapour permeability of earth plasters using small-scale wind tunnels under variable air flow regimes.  
583 *Materials and Structures*, 55(4):110, May 2022.
- 584 [37] EN ISO 17892-4. Geotechnical investigation and testing - Laboratory testing of soil - Part 4:  
585 Determination of particle size distribution. Technical report, 2018.
- 586 [38] NF P94-068. Soils : Investigation and testing - Measuring of the methylene blue adsorption capacity  
587 of a rocky soil - Determination of the methylene blue of a soil by means of the stain test. Technical  
588 report, Association Française de Normalisation, 1998.
- 589 [39] J. J. Fripiat. Surface Properties of Alumino-Silicates. *Clays and Clay Minerals*, 12(1):327–358,  
590 February 1963.
- 591 [40] Matthias Thommes, Katsumi Kaneko, Alexander V. Neimark, James P. Olivier, Francisco  
592 Rodriguez-Reinoso, Jean Rouquerol, and Kenneth S.W. Sing. Physisorption of gases, with special  
593 reference to the evaluation of surface area and pore size distribution (IUPAC Technical Report).  
594 *Pure and Applied Chemistry*, 87(9-10):1051–1069, October 2015.
- 595 [41] Françoise Rouquerol, J. Rouquerol, and K. S. W. Sing. *Adsorption by powders and porous solids:*  
596 *principles, methodology, and applications*. Academic Press, San Diego, 1999.
- 597 [42] Papita Saha and Shamik Chowdhury. Insight Into Adsorption Thermodynamics. In Mizutani  
598 Tadashi, editor, *Thermodynamics*. IntechOpen, Rijeka, 2011. Section: 16.

- 599 [43] Yen-Hua Chen and De-Long Lu. CO<sub>2</sub> capture by kaolinite and its adsorption mechanism. *Applied*  
600 *Clay Science*, 104:221–228, February 2015.
- 601 [44] Yen-Hua Chen and De-Long Lu. Amine modification on kaolinites to enhance CO<sub>2</sub> adsorption.  
602 *Journal of Colloid and Interface Science*, 436:47–51, December 2014.
- 603 [45] G. Gómez-Pozuelo, E. S. Sanz-Pérez, A. Arencibia, P. Pizarro, R. Sanz, and D. P. Serrano. CO<sub>2</sub>  
604 adsorption on amine-functionalized clays. *Microporous and Mesoporous Materials*, 282:38–47, July  
605 2019.
- 606 [46] Lee Stevens, Kimberley Williams, Wong Yoong Han, Trevor Drage, Colin Snape, Joe Wood, and  
607 Jiawei Wang. Preparation and CO<sub>2</sub> adsorption of diamine modified montmorillonite via exfoliation  
608 grafting route. *Chemical Engineering Journal*, 215-216:699–708, January 2013.
- 609 [47] A. Arefi Pour, S. Sharifnia, R. Neishabori Salehi, and M. Ghodrati. Adsorption separation of CO<sub>2</sub>  
610 /CH<sub>4</sub> on the synthesized NaA zeolite shaped with montmorillonite clay in natural gas purification  
611 process. *Journal of Natural Gas Science and Engineering*, 36:630–643, November 2016.
- 612 [48] S. I. Garcés, J. Villarroel-Rocha, K. Sapag, S. A. Korili, and A. Gil. Comparative Study of the  
613 Adsorption Equilibrium of CO<sub>2</sub> on Microporous Commercial Materials at Low Pressures. *Industrial*  
614 *& Engineering Chemistry Research*, 52(20):6785–6793, May 2013.
- 615 [49] Françoise Rouquerol, J. Rouquerol, K. S. W. Sing, P. L. Llewellyn, and G. Maurin. *Adsorption*  
616 *by powders and porous solids: principles, methodology and applications*. Elsevier/AP, Amsterdam,  
617 second edition edition, 2014.
- 618 [50] Robert A. Schoonheydt, Cliff T. Johnston, and Faiza Bergaya. 1 - Clay minerals and their surfaces.  
619 In R. Schoonheydt, C. T. Johnston, and F. Bergaya, editors, *Developments in Clay Science*, volume 9  
620 of *Surface and Interface Chemistry of Clay Minerals*, pages 1–21. Elsevier, January 2018.
- 621 [51] Mustafa A. Alkhabbaz, Praveen Bollini, Guo Shiou Foo, Carsten Sievers, and Christopher W. Jones.  
622 Important Roles of Enthalpic and Entropic Contributions to CO<sub>2</sub> Capture from Simulated Flue  
623 Gas and Ambient Air Using Mesoporous Silica Grafted Amines. *Journal of the American Chemical*  
624 *Society*, 136(38):13170–13173, September 2014.
- 625 [52] F. Wilton Miranda da Silva, Débora A. Soares Maia, Ronan S. Oliveira, Juan Carlos Moreno-  
626 Piraján, Karim Sapag, Célio L. Cavalcante, Giorgio Zgrablich, and Diana C. S. Azevedo. Adsorption  
627 microcalorimetry applied to the characterisation of adsorbents for CO<sub>2</sub> capture. *The Canadian*  
628 *Journal of Chemical Engineering*, 90(6):1372–1380, December 2012.

629 [53] Di Wu, Jeremiah J. Gassensmith, Douglas Gouvêa, Sergey Ushakov, J. Fraser Stoddart, and Alexan-  
630 dra Navrotsky. Direct Calorimetric Measurement of Enthalpy of Adsorption of Carbon Dioxide  
631 on CD-MOF-2, a Green Metal–Organic Framework. *Journal of the American Chemical Society*,  
632 135(18):6790–6793, May 2013.